THE JOURNAL OF PHYSICAL CHEMISTRY C

Article

pubs.acs.org/JPCC

# Exciton Localization and Optical Emission in Aryl-Functionalized Carbon Nanotubes

Brendan J. Gifford,[†,§] Svetlana Kilina,[†] Han Htoon,[§] Stephen K. Doorn,[§] and Sergei Tretiak*[,‡,§]

[†]Department of Chemistry and Biochemistry, North Dakota State University, Fargo, North Dakota 58108, United States

[‡]Theoretical Division, and [§]Center for Integrated Nanotechnologies, Materials Physics and Applications Division, Los Alamos National Laboratory, Los Alamos, New Mexico 87545, United States

Supporting Information

**ABSTRACT:** Recent spectroscopic studies have revealed the appearance of multiple low-energy peaks in the fluorescence of single-walled carbon nanotubes (SWCNTs) upon their covalent functionalization by aryl groups. The photophysical nature of these low energy optical bands is of significant interest in the quest to understand their appearance and to achieve their precise control via chemical modification of SWCNTs. This theoretical study explains the specific energy dependence of emission features introduced in chemically functionalized (6,5) SWCNTs with aryl bromides at different conformations and in various dielectric media. Calculations using density functional theory (DFT) and time dependent DFT (TD-DFT) show that the specific isomer geometry—the relative position of functional groups on the carbon-ring of the nanotube—is critical for controlling the energies and intensities of optical transitions introduced by functionalization, while the dielectric environment and the chemical composition of functional groups play less significant roles. The predominant effects on optical properties as a result of functionalization conformation are rationalized by exciton localization on the surface of the SWCNT near the dopant $sp^3$-defect but not onto the functional group itself.

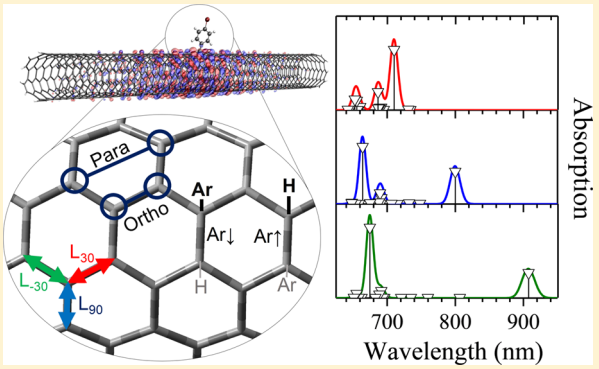


## 1. INTRODUCTION

Single-walled carbon nanotubes (SWCNTs) are nanostructures with unique electronic and optical properties as a result of their one-dimensional (1D) geometry, chirality, and diameter[1,2] and are therefore considered as promising materials for use in modern devices. Covalent functionalization of SWCNTs manipulates the intrinsic electronic properties of SWCNTs beyond what is possible in pristine samples, resulting in the introduction of new optical features.[3,4] These open up a path to several new functionalities including realization of room temperature single photon sources operating at the IR and near IR range[5,6] and increase their utility as active layers in light-emitting technologies.[7−13] Additionally, exciton localization around covalently functionalized SWCNT defect sites[12,14] increases the sensitivity of their optical response in the presence of other chemical species, providing a basis for their use in sensors.[15,16] This promise has resulted in an increased experimental focus in recent years toward preparing SWCNTs that possess sidewall covalent functionalization. Ozonation and solid-state oxidation provide routes for covalent attachment of ether/epoxide[3,14,17,18] groups, while chemical reactions with diazonium salts and halide reagents[4,19,20] result in monovalent and divalent alkyl and aryl groups[21] bound to the nanotube side walls. Although molecular structures of covalently bound functional groups can widely vary, they lead to formation of $sp^3$ defects at the tube surface resulting in a new emission band ($E_{11}$*) at typical energies of 100−300 meV below that of the band-edge exciton $E_{11}$.[3,4,14,15,17−21] The energies of these emission features are extremely sensitive to the defect type[21] and position on the tube[6,22,23] whereas respective photoluminesce (PL) dynamics and efficiency depend on sample preparation, temperature and concentration of the functional groups.[24] Modeling studies have provided some important insights into the nature of these low-energy optical features. For example, a number of computational efforts[12,17,21−23] have focused on simulating absorption spectra for selected binding conformations. In particular, calculations of oxygen bound to (6,5) SWCNTs have shown association of emission peaks with deep trap states tied to different specific chemical species, which agrees with experimental observations.[3,17] Furthermore, large vibronic reorganization energies up to 100 meV have been found between ground and excited states of (6,5) SWCNTs functionalized by aryl groups.[24] Thus, to describe emission, the relaxation energy of the excited state must be introduced into calculations. Finally, sharp emission peaks from individual defect sites spanning a broad wavelength range have been observed in low temperature single nanotube

**Received:** September 26, 2017
**Published:** October 26, 2017




DOI: 10.1021/acs.jpcc.7b09558
J. Phys. Chem. C 2018, 122, 1828−1838

photoluminescence spectroscopy studies in aryl-functionalized (6,5) SWCNTs, introducing the need to understand how the potential for different covalent binding configurations leads to diverse emission features.[6] In spite of the available experimental and theoretical work, a complete understanding of the underlying chemical structure−optical properties relationships is yet to be achieved toward development of full synthetic control of emission behavior.

This current work utilizes density functional theory (DFT) and time dependent DFT (TD-DFT) to optimize the ground and excited state geometries[25] of (6,5) SWCNTs with aryl bromide group functionalization and to explore how a topologically exhaustive set of binding configurations with respect to the SWCNT axis affects both the absorption and emission of SWCNT in the presence of dielectric media. Our calculations demonstrate that substitution of one molecule from two aryl bromides bound to a single carbon ring at the nanotube surface by either H or OH groups has a vanishing effect on the electronic structure and optical response of the functionalized SWCNT. As such, functionalization of the carbon ring of the tube by an aryl derivative and hydrogen is a valid model for the $sp^3$-defect. We further show that the chemical composition of functional groups on the SWCNT plays a much less significant role in governing the energy and intensity of the lowest energy optical transitions than the specific isomer geometry, i.e., the relative position of functional groups on the carbon-ring of the nanotube. Furthermore, the optical transitions are independent of the rotational orientation of the aryl group due to invariance in the electronic structure of the region local to the defect. Because of the nonpolar character of the SWCNT, we also find little dependence of defect-state transition energies on the dielectric environment. We conclude the predominant effects on optical properties as a result of functionalization configuration are due to exciton localization at regions of the SWCNT around the $sp^3$-defect, rather than delocalization onto the functional group. This information is valuable for establishing structure−property relationships and formulating synthetic schemes that optimize desirable optical characteristics for specific applications.

The article is organized as follows: Section 2 describes experimental and computational methodology. Section 3 presents our results. Finally, section 4 summarizes our findings and concludes.

## 2. METHODOLOGY AND COMPUTATIONAL DETAILS

Arylation of aromatic compounds, including SWCNTs,[14,26−28] is frequently achieved using water-soluble aryl diazonium salts. One of the possible scenarios of such a reaction with SWCNTs has been suggested to occur as a two-step reaction.[29] First, the diazonium cation is quickly physisorbed to the outer tube surface. A relatively strong interaction between the nanotube and cation via $\pi-\pi$ stacking allows for electron transfer from the tube to the diazonium molecule forming a charge-transfer transition complex.[22] The complex then decomposes in the rate-limiting step into $N_2$ gas and aryl radical, forming a mixture of covalently and noncovalently bound products, where the large majority of the sample population is attributed to the covalently functionalized SWCNTs by aryl derivatives.[29] Scheme 1 illustrates the plausible carbocation intermediates in this process, where the positive charge on the SWCNT is initially localized on the position adjacent to the site of addition of the aryl group (ortho configuration). Resonance can place this positive charge on the para- site as well. Because of the lack

**Scheme 1. Reaction Mechanism between a SWCNT and Electrophilic Species Generating Reactive Carbocations**

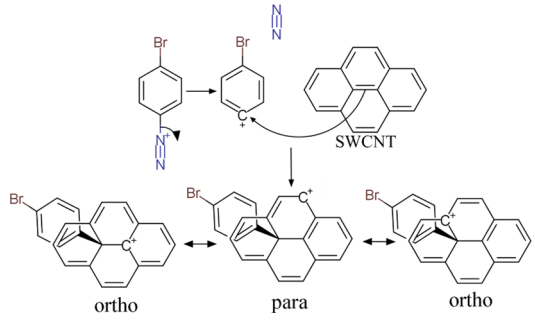


of a resonance structure localizing the positive charge on the meta- site with respect to the aryl attachment, the meta functionalized configuration is not a feasible product following such a reaction mechanism. As such, only ortho and para configurations are considered for this study (Figure 1a). In the

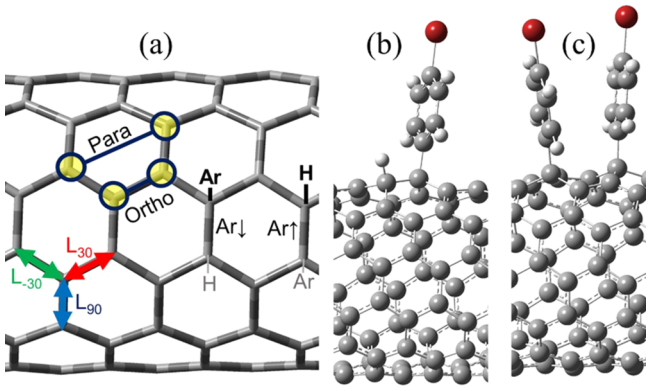


**Figure 1.** Possible orientations of functional groups with respect to the (6,5) SWCNT axis. (a) Ortho denotes functionalization on adjacent carbon atoms, while para refers to functionalization in the (1,4) positions on the same hexagonal ring. $L_{30}$, $L_{90}$, and $L_{-30}$ refers to bonds that lie along a vector 27°, 87°, and −33° from the SWCNT axis, respectively. Ar↑ and Ar↓ refer to the order of functionalization along a chosen vector. Sample representations of a SWCNT functionalized with an aryl bromide group and a hydrogen along the ortho $L_{30}$ bond in the Ar↑ configuration (b) and two aryl bromide groups in the para $L_{30}$ configuration (c).

second step of the reaction between a SWCNT and the diazonium salt, the carbocation intermediate captures a nucleophilic species which could include a second aryl bromide group, hydrogen, or $OH^-$ group (e.g., Figure 1b). All of these adducts are viable choices for SWCNTs in the aqueous environment and therefore aryl-H and diaryl species were considered in this study (Figure 1b,c). We additionally consider the structure in which an H atom is substituted by an OH− group. Only geometries resulting in both reaction sites residing on the same six-membered ring are considered, since our previous investigations show that these are the only species that exhibit optically active transitions.[23,22] Any binding configurations other than these lead to unpaired reactive electron(s) and, as a consequence, a gap-less continuous density of excited electronic states, which invalidates formation of optically active quantum states.

In addition to variable distance between reaction sites and species, the resonance depicted in Scheme 1 can result in


DOI: 10.1021/acs.jpcc.7b09558
J. Phys. Chem. C 2018, 122, 1828−1838

products functionalized along three distinct bonding directions with respect to the SWCNT axis. Figure 1a depicts these directions, corresponding to the different bonds of the SWCNT hexagonal lattice, labeled as $L_{30}$, $L_{90}$, and $L_{-30}$, where the subscript describes the approximate angle between a vector lying along the bond and the SWCNT axis. In the case of the (6,5) SWCNT explored here, these angles are more precisely 27°, 87°, and −33° for $L_{30}$, $L_{90}$, and $L_{-30}$, respectively. One further structural modification that must be acknowledged is the possibility for the interchange of the two functional sites on the SWCNT. Swapping two similar functional sites (two aryl groups, referred to as diaryl) for nonequivalent functional pairs, such as aryl- and H-groups (referred to as aryl-H), results in distinct geometries. Viewing a (6,5) SWCNT in a perspective that results in a horizontal tube axis allows every carbon atom to either reside at the "top" or the "bottom" of a hexagonal ring. Therefore, either the top or the bottom of the hexagonal ring is functionalized with an aryl group to generate "Ar↑" and "Ar↓" configurations, respectively, as shown in Figure 1. The remaining position is functionalized with the opposing species. It is notable that through considering this interchange, this study implicitly considers the differences between the functionalization of left- and right-handed SWCNT. Considering all these possible structure modifications results in 12 distinct aryl-H and 6 distinct diaryl configurations.

The pristine SWCNT was created with (6,5) chirality to a length of ∼12 nm by generating 3 unit cells with Tubgen 3.4 software.[30] To fulfill the vacancies of all terminal carbon atoms, the ends of the SWCNT were capped with hydrogen atoms in all positions according to the capping scheme reported previously.[31,32] The geometry of the pristine SWCNT was then optimized sequentially by first using UFF[33] molecular mechanics followed by AM1[34] semiempirics, and finally density functional theory (DFT) with a CAM-B3LYP[35] functional and 3-21G basis set in vacuum. This methodology has been shown to be in reasonable agreement with experimental data.[36,37] Once the pristine SWCNT geometry was optimized, this structure was then functionalized in the positions previously described. To generate the starting geometries, the torsion angle between the SWCNT and aryl group was adjusted such that the plane containing all the atoms in the aryl group and a vector connecting the SWCNT carbon atoms vicinal to each functional group were perpendicular, Figure 1, parts b and c. The resulting functionalized SWCNTs were then optimized using the same stepwise methodology previously described. All geometry optimizations were performed using Gaussian-09, version E.01 software.[38] The resulting geometries were utilized as starting points for geometry optimization in the dielectric environment of three solvents of increasing polarity including heptane ($\varepsilon$ = 1.9113), acetonitrile ($\varepsilon$ = 35.688), and water ($\varepsilon$ = 78.3553). The effect of the solvent was introduced implicitly using the conductor-like polarizable continuum model (CPCM)[39] as implemented in Gaussian-09. Because of the negligible difference between both the geometry and relative energetics of the optimized geometries in vacuum and solvent (Table S3), the excited state calculations were performed using those structures optimized in vacuum.

The molecular orbitals (MOs) for the resulting geometries of both pristine and aryl-functionalized SWCNTs were generated using CAM-B3LYP functional and 3-21G basis set and visualized by applying isosurface with an isovalue of 0.008 using Visual Molecular Dynamics (VMD) software.[36] The results are also compared to those calculated by STO-3G basis set. To simulate the optical characteristics, the vertical excitations for 15 states were calculated using TD-DFT using the ground state optimized geometries in vacuum and then recalculated in the dielectric environment of the three solvents. The profiles of absorption spectra were generated by broadening about the optical transitions using a Gaussian function of line width 0.01 eV weighted by the oscillator strength of the transition. To obtain the fluorescence spectra, the excited-state geometry is optimized,[25] whereby the lowest singlet excitation energy is calculated within the linear response theory framework.[40] Both the absorption and emission spectra calculations were performed using the same functional and basis set as for the geometry optimization. Natural transition orbital (NTO) analysis[41] was then performed to obtain the electron−hole pairs of monoelectron orbitals that contribute to each optically active transition of a specific excited state, as implemented in Gaussian-09 software.

## 3. RESULTS AND DISCUSSION

**3.1. Relative Stabilities and Geometries of Binding Configurations.** Different functionalizations of SWCNTs with an aryl derivative and hydrogen result in similar total energies for all Ar↑ and Ar↓ configurations considered (shown in Figure S1 in the Supporting Information). The observed difference between the total energies of Ar↑ and Ar↓ indicates that these structures are indistinguishable at normal conditions. Assuming the absence of environmental effects such as the presence of surfactants, this indicates the aryl functionalization provides no selectivity between the left- and right-handed (6,5) SWCNT. The differences in total energies between various ortho and para isomers of aryl-H configurations are more noticeable, with all computed energies falling within a 0.1−0.4 eV range from the most stable ortho $L_{-30}$ configuration, Figure 2a. When both functional groups are the same in diaryl structures, the most stable configuration becomes para $L_{90}$, being different from ortho $L_{-30}$ by ∼0.05 eV, while the energy difference range

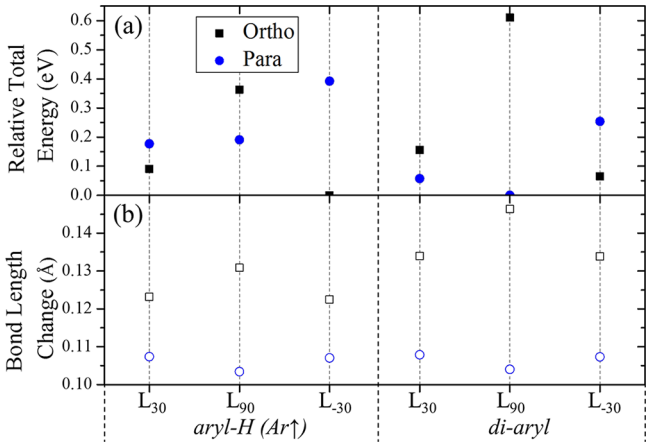


**Figure 2.** Dependence of structural and energetic changes on the functional group conformation calculated in vacuum using CAM-B3LYP functional and 3-21G basis set. (a) Relative total energies of functionalized isomers with respect to the most stable structure compared between (6,5) SWCNT functionalized with an aryl bromide group and a hydrogen (aryl-H) and two aryl bromide groups (diaryl). (b) Averaged difference between carbon−carbon bond lengths adjacent to aryl functionalization and those in the pristine SWCNT. Black squares represent ortho configurations, while blue circles represent para configurations.



DOI: 10.1021/acs.jpcc.7b09558
J. Phys. Chem. C 2018, 122, 1828−1838

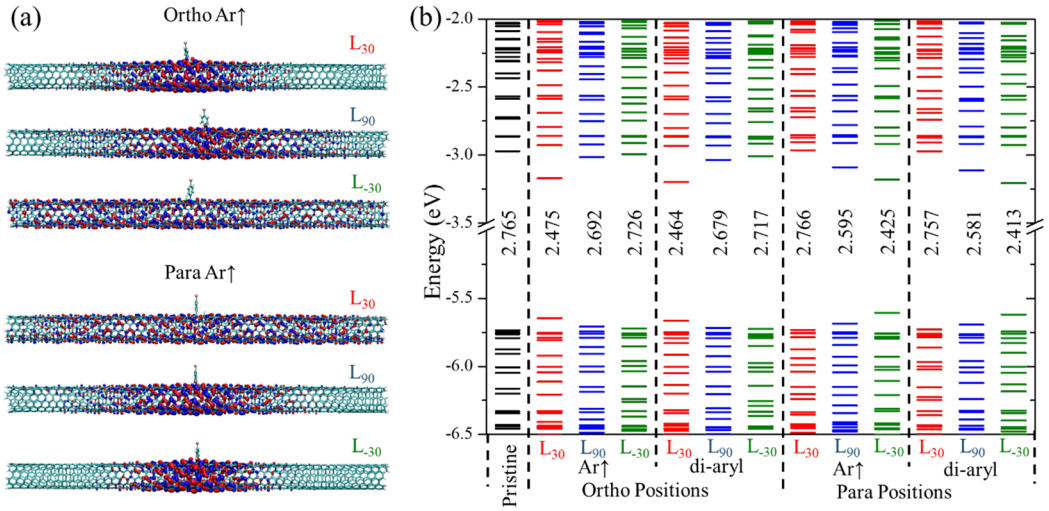


**Figure 3.** Ground state electronic structure comparing Ar↑ aryl-H and diaryl funtionalized (6,5) SWCNT in vacuum. Highest occupied molecular orbitals (HOMOs) (a) and the electronic level diagram (b) for functional groups bounded along a vector 27° ($L_{30}$), 87° ($L_{90}$), and −33° ($L_{-30}$) from the SWCNT axis. The values placed between the HOMO and LUMO are the HOMO−LUMO gaps in eV.

between all ortho and para isomer structures varies from 0.05 to 0.6 eV, Figure 2a. In general, binding with the second aryl group instead of hydrogen slightly increases the total energies of all ortho configurations, while it also weakly stabilizes the para conformations, although the changes are relatively small in all cases.

Note that an increase in the basis set size, from STO-3G to 3-21G, somewhat reduces the energies of the para configurations, while the energy of ortho structures insignificantly change both in aryl-H and diaryl structures, Figure S2 and Table 1 in Supporting Information. Overall, an increase in the basis set has a qualitatively minor effect on both the geometry and the electronic structure (Figure S3 in Supporting Information), which agrees with conclusions from previous literature reports.[37,42] In particular, prior calculations of OH-functionalized (9,0) nanotubes using B3LYP/3-21G show a maximum of 0.3% difference in bond lengths compared to B3LYP/6-31G* results.[42] Our calculations show that increasing the basis set from STO-3G to 3-21G uniformly redshifts the energy gap and excitation energies by a maximum of about 0.2 eV, regardless of isomer geometries, Figure S4 in Supporting Information. In our previous work,[36,37] we have shown that a further increase of the basis to 6-31G and 6-31G* insignificantly affects optical transitions of pristine nanotubes. Thus, the qualitative physical picture obtained from our calculations is not affected by the methodology. Overall, the difference in total energies of the isomer configurations of functionalized SWCNTs is due to the local disruption of the $sp^2$-hybridization in the region of functionalization, as well as the resulting effects on electron delocalization across the entire system.

For ortho configurations, the bond lengths adjacent to the aryl functional group are elongated significantly more than for para configurations, Figure 2b. In these cases, the greatest elongation is observed along the axis of functionalization due to the concurrent disruption of the $sp^2$-hybridization of the carbon atom in that direction. The remaining two bonds become lengthened over the pristine SWCNT to a similar degree (Table S2 in Supporting Information) leading to the $sp^3$-defect at the conjugated structure of the nanotube. Figure 2b shows that the average bond disruption is the most significant for ortho functionalization along $L_{90}$, coinciding with the highest energy among ortho structures, Figure 2(a). Additionally, the disruption of $sp^2$ hybridization is observed to be greater in diaryl-functionalized SWCNTs than for aryl-H functionalization. This is accompanied by the corresponding increase in the total energies for all ortho functionalized species. In contrast, para configurations exhibit significantly less elongation of bond lengths, indicating a lower degree of $sp^2$ disruption in the region local to functionalization for both aryl-H and diaryl structures. Additionally, the smaller elongation is nearly uniform across all para-isomers, which coincides with a consistent energy difference between the various para configurations (≤0.2 eV), as compared to those of the ortho structures (up to 0.6 eV). However, the smaller degree of $sp^2$ distortion does not always provide the lowest energy configuration, resulting in para isomers having in most cases larger energy than ortho isomers, except for $L_{90}$, where ortho structures have significant changes in the bond lengths. Thus, some moderate $sp^2$ distortion, like in the ortho $L_{-30}$ configuration, efficiently stabilizes both aryl-H and diaryl structures.

It seems reasonable to suggest that computation of a larger number of unit cells in the SWCNT model, covered with a similar number of functional sites (i.e., modeling a lower concentration of functionalization), might yield an even smaller energy difference between various functionalization geometries. As such, it would be inappropriate to conclude that the ortho $L_{-30}$ for aryl-H and para $L_{90}$ for diaryl are the most thermodynamically probable configurations of the defect position for (6,5) nanotube samples. Additionally, absent from these considerations is the kinetic component, which is driven by thermal fluctuations and is affected by solvent and surfactant molecules covering the tube surface. The latter affects collisions between molecules during the dissociation reaction of diazonium salts into $N_2$ gas and aryl radical forming a mixture of covalently and noncovalently bound products.[29] Since it is known that aryl diazonium salts have very complicated chemistry in solutions due to the variety of reaction pathways with a large number of potential intermediate products, we assume that all 12 aryl-H or six diaryl isomers can coexist in experimental samples.



DOI: 10.1021/acs.jpcc.7b09558
J. Phys. Chem. C 2018, 122, 1828−1838

The geometry optimizations performed in the different dielectric environment of solvents ranging from the nonpolar heptane to very polar water results in no noticeable structural and energetic difference between defect conformations (Figure S5 and Table S3 in the Supporting Information). This can be rationalized by the nonpolar character of the nanotube, while different isomer conformations of polar functional groups result in a small electrostatic dipole moment of the entire system (≤1 D) in all solvents. While the total electrostatic dipole moment of the functionalized nanotubes increases with the solvent polarity (by 0.1−0.3 D), its relative change between the different conformations stays nearly the same (Figure S6 and Table S3 in the Supporting Information), which explains the insensitivity of the defect conformations to the solvent. As such, any difference in properties of aryl-functionalized SWCNT samples observed in different solvents is likely not due to structural changes induced by the environment, but can be associated with a different response of the intrinsic electronic structure that is expected to be more sensitive to dielectric effects.

**3.2. Binding Configuration and Electronic Structure.** The electron localization in the frontier molecular orbital in the vicinity of the defect plays a significant role in modulating the precise energetics of the orbitals and therefore the gap between the highest occupied molecular orbital (HOMO) and lowest unoccupied molecular orbital (LUMO).[32] For example, the HOMO (and LUMO) of the para $L_{30}$ species exhibits electron delocalization along the entire axis of the SWCNT and the largest energy gap among para isomers for both aryl-H and diaryl structures, Figure 3. In contrast, the para $L_{-30}$ species shows significant orbital localization around the defect site and the smallest energy gap for para isomers calculated in vacuum, Figure 3. For the ortho isomer, the trend is opposite, showing the most delocalized frontier orbitals for $L_{-30}$ and having the largest energy gap, while $L_{30}$ exhibits the most localized orbitals and the smallest energy gap among all ortho structures. $L_{90}$ is in the intermediate range of orbital delocalization and the HOMO−LUMO energy for both ortho and para structures. Overall, the degree of electron localization/delocalization correlates well with the trends of the energy gap and almost perfectly mirrors ortho $L_{30}$, $L_{90}$, and $L_{-30}$ to para $L_{-30}$, $L_{90}$, and $L_{30}$, where the lowest HOMO−LUMO gap and the strongest orbital localization is observed for ortho $L_{30}$ and para $L_{-30}$, while the largest energy gap and the largest degree of delocalization corresponds to ortho $L_{-30}$ and para $L_{30}$.

All these trends are identical for both aryl-H and diaryl structures. Moreover, the substitution of H by an OH group results in no noticeable changes in the electronic structure of the functionalized SWCNTs, Figure S7 in Supporting Information. It is important to note that even for strongly localized orbitals, the charge density is spread over the part of the tube around the defect site rather than localized on the functional group. This feature of orbital localization underscores the insensitivity of the frontier molecular orbitals of the SWCNT to the chemical composition of the second functional group attached to the same carbon-ring of the tube as the aryl bromide. The position of the functional groups plays a predominant role in governing the electronic structure, while chemical composition of the functional group is secondary.

Overall, all functionalized SWCNTs have a smaller energy gap than the pristine (6,5) nanotube, Figure 3(b). Isomer structures with the highest degree of HOMO and LUMO delocalization (ortho $L_{-30}$ and para $L_{30}$) exhibit only slight differences from the energy gap of the pristine tube, while conformations with highly localized character of their frontier orbitals (ortho $L_{30}$ and para $L_{-30}$) have a significantly reduced HOMO−LUMO gap. For a hypothetical infinite-length SWCNT, it is expected that the HOMO and LUMO would exhibit double degeneracy. Slight deviation from this expectation is shown in the computations of the pristine (6,5) system, likely due to end-group effects, Figure S8 in Supporting Information. However, the $sp^3$-defect in the functionalized nanotube completely lifts this degeneracy, resulting in a large splitting between the HOMO and HOMO−1 and LUMO and LUMO+1. As a result, the HOMO is destabilized and the LUMO is stabilized, which decreases the HOMO−LUMO gap in all functionalized structures compared to the pristine tube, which is the most pronounced in isomers having more localized character in their frontier orbitals around the defect site.

**3.3. Optical Properties Arising from Distinct Binding Configurations.** The dependence of the ground state electronic structure on the $sp^3$-defect position also governs the optical properties of functionalized (6,5) nanotubes, as illustrated in Figure 4. In the absorption spectrum of the pristine nanotube calculated in vacuum, the lowest energy peak is observed at ∼700 nm, with the main contribution being from the optically active $\pi \rightarrow \pi^*$ transitions (states 5 and 6 in Figure 4a). Here NTOs demonstrate exciton density delocalized across the entire length of the SWCNT, Figure 5. This peak is assigned to the $E_{11}$ band. Note that the energy of $E_{11}$ is expected to be blue-shifted compared to the experimental peaks, due to unphysical density functional, limited basis set,

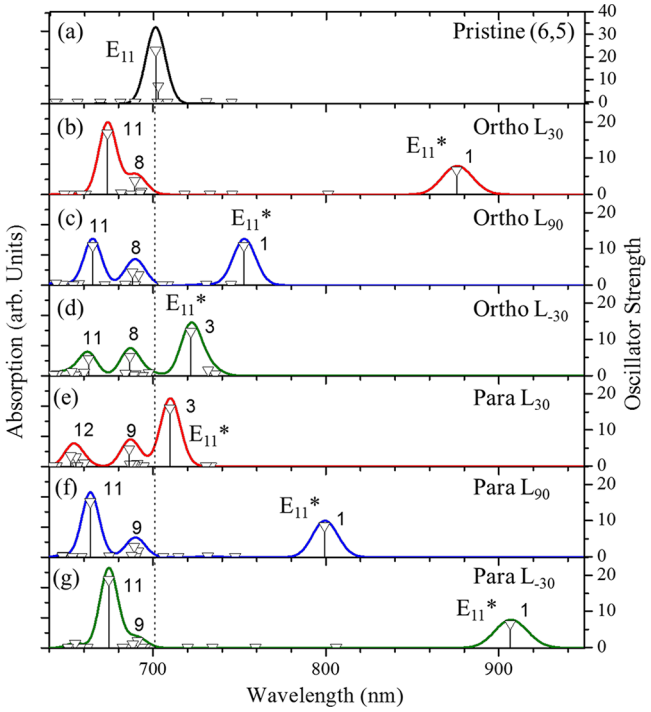


**Figure 4.** Absorption spectra of the pristine (6,5) SWCNT (a), and its functionalized counterpart in ortho $L_{30}$ (b), ortho $L_{90}$ (c), ortho $L_{-30}$ (d), para $L_{30}$ (e), para $L_{90}$ (f), and para $L_{-30}$ (g) Ar↑ conformations calculated in vacuum. The vertical black lines correspond to the optical transitions with the height related to their oscillator strength, which values are shown at the right *Y*-axis. The dashed line indicates the reference point for the energy of the $E_{11}$ transition in the pristine SWCNT.



DOI: 10.1021/acs.jpcc.7b09558
J. Phys. Chem. C 2018, 122, 1828−1838

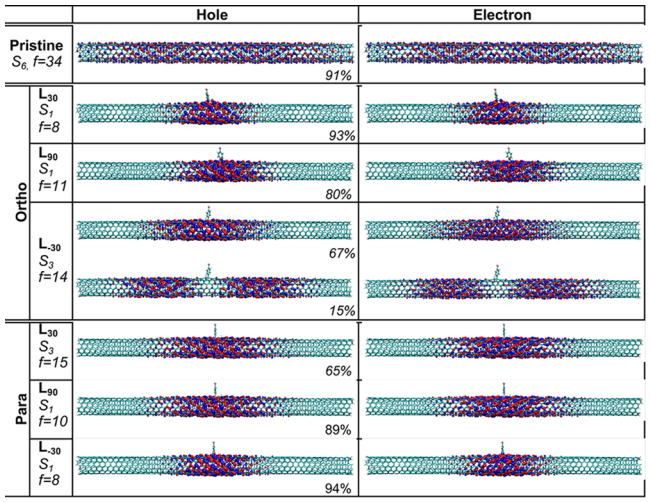


**Figure 5.** Natural transition orbitals (NTOs) representing the photoexcited electron−hole pair contributing to the brightest transitions in the lowest energy $E_{11}$* absorption band of aryl-H (Ar↑) structures and compared to the brightest transition in the $E_{11}$ absorption band of pristine (6,5) SWCNT in vacuum. The left column presents information on the transition number and its oscillator strength (also see Figure 4). Only the NTO pairs that mostly contribute to the transition are shown, with the percent of their contribution depicted at the bottom of each NTO image.

and the confinement effect of the finite-size tube model.[36] Functionalization introduces new defect-based optical transitions at much lower energy ranges from the original $E_{11}$ band (labeled $E_{11}$* in Figure 4). The degree of red shifts of $E_{11}$* from $E_{11}$ bands depends on the precise position of the $sp^3$-defect, following the trends in their ground state energy gaps. Thus, the greatest red shifts are observed for para $L_{-30}$ and ortho $L_{30}$, followed by para $L_{90}$ and ortho $L_{90}$, Figure 4, parts b, g and parts c, f, respectively. For these isomer conformations, the lowest-energy transition is optically active and originates predominantly from the transition between the HOMO and LUMO, demonstrating noticeable localization of NTOs around the defect site, Figure 5.

Conversely, only slight red shifts in the lowest energy absorption peaks are observed for ortho $L_{-30}$ and para $L_{30}$, Figure 4, parts d and e. In these cases, however, the first two lowest energy transitions are optically forbidden (dark states), similar to the pristine nanotube. These dark transitions have highly delocalized $\pi \rightarrow \pi^*$ character, with the orbital density spread over the tube surface, but with some slight preferential localization over one side of the tube with respect to the defect, Figure S9. We suggest this preferential localization over one side of the nanotube is due to the asymmetry of the defect position, which is not located directly at the middle of the tube. This asymmetry in the geometry translates to the excited state orbitals. The NTOs contributing to the optically active lowest-energy $E_{11}$* band (transition 3 in Figure 4, parts d and e) of ortho $L_{-30}$ and para $L_{30}$ exhibit localization around the defect site, similar to the optically allowed $S_1$ transitions in other isomer conformations, Figure 5. However, in comparing this $S_3$ exciton to the strongly red-shifted and optically active $S_1$ states in para $L_{30}$ and ortho $L_{-30}$, one can notice its higher degree of delocalization. Enhanced delocalization of the $S_3$ excitonic state in ortho $L_{-30}$ and para $L_{30}$ also correlates with its slightly "brighter" nature (higher oscillator strength), than $S_1$ in para $L_{30}$ and ortho $L_{-30}$ having more pronounced localization around the defect site.

Highly delocalized NTOs are observed for bright transitions at the higher-energy band for all isomer configurations (transitions 8−12 in Figure 4), as illustrated in Figures S10 and S11 in the Supporting Information. We assign these transitions to the main $E_{11}$ band because of their completely delocalized $\pi \rightarrow \pi^*$ character similar to those in pristine SWCNT. However, the functionalization splits $E_{11}$ into two less intense and blue-shifted peaks, compared to the $E_{11}$ band in the pristine nanotube, Figure 4. The degree of this splitting and relative intensity of peaks in the $E_{11}$ band depends on the defect position. The least blue-shifted peak in $E_{11}$ formed by transitions $S_8$ and $S_9$ has its energy and intensity nearly independent of the isomer conformations. This can be rationalized by their NTOs being delocalized over the entire tube but having a node at the defect position, Figure S10 in Supporting Information. Because the exciton density has minimal contribution from the defect site, the energy of these transitions is not so much affected by the isomer geometries. Conversely, the excitons in the most blue-shifted peak in the $E_{11}$ band ($S_{11}$ and $S_{12}$) have two nodes and three maxima in their density around the defect site and close to the tube edges, making the energy and intensity of these transitions more sensitive to the isomer conformations, as well as to the edge effects. The nodal structure of excitons originates from the wave function confinement due to the finite-size tube model. This nodal structure has the same physical meaning as a characteristic standing wave feature related to its k-vector.[36,43] Thus, the delocalized excited states can be considered as standing waves in quasi-1D structures,[44] where the nodes are related to the exciton momenta, k. Consequently, the zero-node state is associated with the $k = 0$ exciton in the infinite nanotube limit, which has stronger interaction with the defect at the tube center causing its dramatic red shift. States having one or more nodes belong to the same excitonic band as the respective zero-node exciton, but have higher values of the momentum and higher energies.

**3.4. Optical Properties and Rotational Conformation of Functional Groups.** Since the lowest energy optical transitions in functionalized SWCNT are localized around the defect site, it is imperative to determine the degree of interaction between the electron density located on the SWCNT near the defect and the electron density on the defect itself and also find how this interaction affects optical properties. This interaction is expected to have some dependence on the precise rotational position of the aryl group with respect to the SWCNT axis. To explore this effect, the potential energy surface (PES) at different rotation angles about the C−C bond between the aryl group and SWCNT were calculated along with the absorption spectra of aryl-H isomers with the aryl bromide conformations corresponding to the minimal and maximal energies along this PES, see Figure S12 and discussion in Supporting Information. The absorption spectra obtained for these different geometries in either the minimum or maximum of the PES, are nearly identical. As such, the overlap between the exciton density in the $\pi$-systems of the SWCNT and the aryl group has negligible effect on the optical properties. This observation further validates the relative similarities of electronic structures between aryl-H, aryl-OH, and diaryl systems.

**3.5. Solvent Effects and Optical Properties.** Computation of the excitation energies in a dielectric environment of



DOI: 10.1021/acs.jpcc.7b09558
J. Phys. Chem. C 2018, 122, 1828−1838

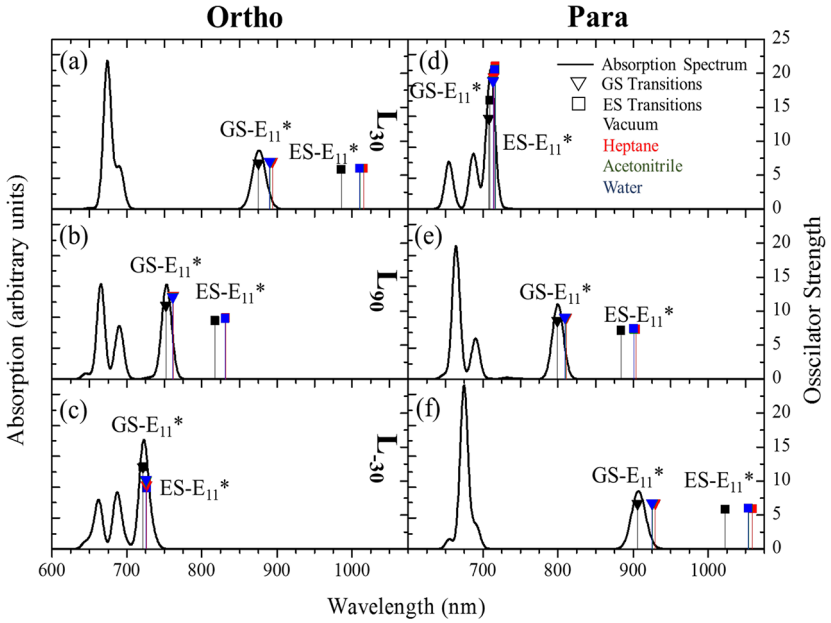


**Figure 6.** Absorption and emission transitions of the Ar–H isomers calculated in various solvents: (a) ortho $L_{30}$, (b) ortho $L_{90}$, (c) ortho $L_{-30}$, (d) para $L_{30}$, (e) para $L_{30}$, and (f) para $L_{-30}$ configurations. The black curves are absorption spectra in vacuum. Vertical lines with symbols of black, red, green, and blue colors represent the lower energy optically active transitions in the $E_{11}$* band of functionalized SWCNTs in vacuum, heptane, acetonitrile, and water, respectively. The height of the vertical lines corresponds to the values of the oscillator strength of these transitions, shown at the right *Y*-axis. Triangles depict the lowest energy transitions contributing to the absorption (calculated at the ground state, GS, geometry) and squares the emission (calculated at the optimized excited state, ES, geometry).

increasing polarity reveals small bathochromic shifts for all the structures we studied, Figure 6. The $E_{11}$ absorption band of the pristine (6,5) SWCNT exhibits a red shift of ∼30 meV when computed in hexane versus vacuum, Figure S13(a) in the Supporting Information. However, increasing the polarity of the solvent over the wide range of $\varepsilon$ = 1.9 for hexane to $\varepsilon$ = 78.4 for water only results in a slight increase of the energy of optical transitions, while acetonitrile ($\varepsilon$ = 35.7) as solvent has a similar effect on transitions as water. Identical trends are observed for the $E_{11}$ absorption band of all functionalized nanotubes, where the maximal shifts are not more than 30 meV in ortho $L_{30}$ and para $L_{-30}$ structures, and are nearly zero for ortho $L_{-30}$ and para $L_{30}$ isomers.

Likewise, the bathochromic shifts for the $E_{11}$* absorption band of all functionalized nanotubes are also found to be small on comparing spectra in vacuum and water, with the largest shifts of ∼40 meV corresponding to the $E_{11}$* of ortho $L_{30}$ and para $L_{-30}$, while nearly no shifts of $E_{11}$* are found with respect to the main $E_{11}$ band for ortho $L_{-30}$ and para $L_{30}$ isomers, Figure 6. This negligible solvent effect can be attributed to the relatively low electrostatic dipole moments of these systems. For all species, the calculated static dipoles are less than 0.6 D, with the smallest dipole moments of ortho $L_{-30}$ and para $L_{30}$ configurations (Figure S6 and Table S3 in Supporting Information) exhibiting diminishing bathochromic shifts. As such, only small perturbations in electronic structure and optical properties are observed as the result of the dipole–dipole interactions with the environment. These results coincide with our previous studies of (6,2) SWCNT covalently functionalized by aryls that have also shown negligible solvent effects on the absorption spectra of functionalized SWCNT.[22]

Energetic trends in emission features of the functionalized (6,5) SWCNTs in vacuum and solvent are consistent with those of the lowest energy absorption band $E_{11}$*, while showing just slightly more pronounced bathochromic shifts. The magnitude of the bathochromic shifts of the emission energy in different solvents also depends on the defect configuration in the same way as for the transitions in the $E_{11}$* absorption band, Figure 6. The mirroring trends between the $E_{11}$* absorption band and the emission states justifies that calculations of the lowest states in absorption spectra provide a qualitatively correct description of the PL in SWCNTs and functionalized SWCNTs.

While the trends in absolute energies of absorption and emission have been shown to be identical, the Stokes shifts fall in the range between 5 and 168 meV, depending on the defect conformation, and follow similar trends as found for the bathochromic shifts in varying solvents. Negligible Stokes shifts are found for the ortho $L_{-30}$ and para $L_{30}$ configurations, which also display the least red-shifted emission energies with solvent. Conversely, the largest Stokes shifts are found for the ortho $L_{30}$ and para $L_{-30}$ configurations, which have the most red-shifted emission. Substantial values of Stokes shifts in the presence of ortho $L_{30}$ and para $L_{-30}$ defects can be understood in terms of vibrational reorganization due to deformation of the nanotube geometry upon exciton trapping at the defect site upon photoexcitation.[24] Thus, NTOs contributing to the emission states demonstrate similar character as that found for the lowest energy excitons in the $E_{11}$* absorption band, but with enhanced localization around the tube center for both pristine and functionalized SWCNTs, as illustrated in Figure 7. Emission states for the ortho $L_{-30}$ and para $L_{30}$ configurations show a low degree of exciton localization around the defect site. The NTOs contributing to the $E_{11}$* absorption band for these species show a delocalization pattern similar to those of the pristine tube, rationalizing the negligibly small Stokes shifts in these systems. In contrast, ortho $L_{30}$ and para $L_{-30}$ structures show noticeably increased localization around the defect site, compared to their excitons in the $E_{11}$* absorption band and, consequently, have the largest Stokes shifts. Such a substantial vibrational


DOI: 10.1021/acs.jpcc.7b09558
J. Phys. Chem. C 2018, 122, 1828–1838

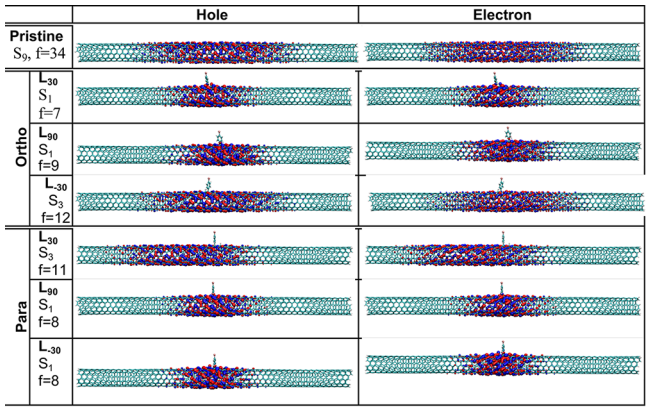


**Figure 7.** Natural transition orbitals (NTOs) representing the photoexcited electron−hole pair contributing to the lowest energy emission state of aryl-H (Ar↑) structures and compared to the emission state of pristine (6,5) SWCNT in vacuum. The left column represents information on the state number and its oscillator strength. Only the NTO pairs that dominantly contribute to the transition (>60%) are shown.

reorganization energy between the excited and ground state of SWCNTs in the presence of a fluorescent defect agrees well with experimental[24] and computational[24] reports for (6,5) SWCNTs functionalized with various aryl derivatives.[24]

Similar to the absorption results, the ortho $L_{-30}$ and para $L_{30}$ configurations with the least red-shifted emission energies have two optically dark lowest energy states with the third state being emitting. Therefore, the emission of these isomers is expected to be the least intense among all other defect conformations due to the "trapping" of the excitation in the optically inactive lowest energy states. However, this weakly emissive peak is close in energy to the $E_{11}$ main band and, therefore, would be hard to resolve in experimental samples. In contrast, the most red-shifted emission states from ortho $L_{30}$ and para $L_{-30}$ are expected to be significantly distinct from the emission peaks associated with the ortho $L_{90}$ and para $L_{90}$ conformations. As such, the experimental photoluminescence (PL) spectra of functionalized (6,5) SWCNTs, where defects associated with aryl bromide groups are naturally present in various isomer conformations, is expected to have several well-pronounced emission features. These correspond to the most red-shifted $E_{11}$* band of ortho $L_{30}$ and para $L_{-30}$, followed by the less red-shifted $E_{11}$* bands of $L_{90}$ and para $L_{90}$, and the wide main $E_{11}$ band close in its energy to the $E_{11}$ band or the pristine SWCNT. These theoretical predictions agree well with recent experimental data.[6]

## 4. CONCLUSIONS

Synthetic considerations dictate that covalent functionalization of SWCNTs must produce more than one defect site, and computations require at least two carbon atoms at the SWCNT surface be functionalized in order to avoid the formation of open-shell or charged systems. Such functionalization can occur along three distinct directions with respect to the defect site and at either ortho or para positions on a single ring. Our calculations show that all isomers arising from different binding positions of the covalently bound aryl bromides at a single carbon-ring of the (6,5) SWCNTs result in significant distortion of the $sp^2$-conjugation of the SWCNT and formation of an $sp^3$-defect on the nanotube surface. The largest disruption of the hexagonal $sp^2$-hybridized network from the pristine SWCNT occurs between the two functional sites oriented along bonds nearly perpendicular to the nanotube axis, $L_{90}$, for ortho functionalization leading to the highest total energy of these conformations. All para configurations exhibit a noticeably lower degree of $sp^2$ disruption than do ortho isomers. However, a smaller degree of $sp^2$ distortion does not always provide the most stable configuration, typically resulting in para isomers having higher total energy than ortho isomers. We conclude that a moderate $sp^2$ distortion, like in ortho $L_{-30}$ and ortho $L_{30}$, is optimal for stabilization of structures. Nonetheless, the energy differences between all these functional conformations are relatively low, indicating the plausibility of coexistence of several different defect geometries in experimental samples.

Substitution of one molecule from two aryl bromides bound to a single carbon ring at the nanotube surface by either H or $OH^-$ groups has very similar effects on the electronic structure and optical response of the functionalized SWCNT. This is rationalized by the fact that the ground and excited state orbitals associated with the defect completely originate from the SWCNT, rather than from the functional group itself. By the same reason, the rotation of the aryl group about the C−C bond with respect to the nanotube also has negligible effect on the optical spectrum of the system. Overall, functionalization of the carbon ring of the nanotube by an aryl derivative and hydrogen is a valid model for the $sp^3$-defect on the tube surface. Swapping of the position of the aryl group and hydrogen atom to the "top" or the "bottom" of the hexagonal ring of the nanotube leaves the total energies and electronic structure of functionalized SWCNTs virtually unchanged. Thus, these structures are indistinguishable at normal conditions, which means that the aryl functionalization does not provide any selectivity between the left- and right-handed (6,5) SWCNT absent the effects of surfactants.

While the chemical composition (-H, -OH, -aryl) of the functional group bound to the second carbon position of the carbon ring being considered has less effect on the photophysical properties of the nanotube, the energy and intensity of the lowest energy optical transitions are very sensitive to the specific isomer geometry. Thus, the appearance of the red-shifted optically allowed $E_{11}$* band in absorption spectra of the functionalized SWCNTs is the result of excition localization around the $sp^3$ defect, which determines the degree to which the lower energy excitons depend on the defect conformation. The isomers having the strongest localization of their frontier orbitals around the defect exhibit the largest redshifts of their $E_{11}$* band, while structures with a smaller degree of orbital localization have the least redshift of the $E_{11}$* peak, with respect to the main $E_{11}$ band of the pristine SWCNT. Optically active excitons contributing to these peaks are delocalized over the entire nanotube, but have nodes either at the defect position or in-between the defect and the nanotube edges. Such a nodal structure for the excitons has the same physical meaning as a characteristic standing wave feature related to its *k*-vector in the infinitely long quasi-1D nanotube. This demonstrates that both $E_{11}$ and $E_{11}$* bands in functionalized nanotubes are derivatives of the lower energy bright $E_{11}$ excitonic band of the pristine SWCNT.

Solvent effects present another important factor potentially affecting emission energies. Very small bathochromic shifts of $E_{11}$* (up to ∼40 meV) and $E_{11}$ (up to ∼30 meV) are observed for both absorption and emission due to the very small electrostatic dipole moments present in the functionalized SWCNTs. Relaxation of the excited state enhances electron and


DOI: 10.1021/acs.jpcc.7b09558
J. Phys. Chem. C 2018, 122, 1828−1838

hole localization around the tube center for both pristine and functionalized SWCNTs. The higher the degree of exciton trapping at the defect site the larger is the Stokes shift (ranging from 5 to 168 meV), following similar trends as for the bathochromic shifts in varying solvents. Therefore, the largest Stokes shifts are observed in the isomers having the most red-shifted emission with the most localized character of their excited charge densities (ortho $L_{30}$ and para $L_{-30}$), while cases of negligible Stokes shifts correspond to configurations having the least red-shifted emission energies and the most delocalized excitonic orbitals (ortho $L_{-30}$ and para $L_{30}$). This trend is rationalized by occurrence of a more pronounced difference in the excitonic states upon excited state relaxation in ortho $L_{30}$ and para $L_{-30}$ than for ortho $L_{-30}$ and para $L_{30}$ isomers. Despite substantial vibrational reorganization between the excited and ground state of SWCNTs in the presence of a fluorescent defect, we have observed the mirroring trends between the $E_{11}$* absorption band and the lowest energy emission states for all defect conformations. This justifies that calculations of the lowest states in absorption spectra provide qualitatively correct descriptions of the PL in both SWCNTs and functionalized SWCNTs. Thus, for saving computational time, the optimization of the excited state can be omitted and conclusions on the trends in emission transitions can be made based from the lowest energy absorption peak. Furthermore, for reduced computational expense, use of a small basis set (e.g., STO-3G) is justified, since numerically expensive simulations using the larger 3-21G basis produces the same trends across all calculated observables apart from uniform red-shifts (~0.2 eV) for optical transition energies.

Finally, our calculations predict that in nanotube samples where defects associated with aryl bromide groups are naturally present in the various available isomer conformations, the PL spectra of functionalized (6,5) SWCNTs are expected to exhibit three well pronounced emissive peaks: the most red-shifted $E_{11}$* band of ortho $L_{30}$ and para $L_{-30}$, followed by the less red-shifted $E_{11}$* band of $L_{90}$ and para $L_{90}$, and the wide main $E_{11}$ band mixed with $E_{11}$* of ortho $L_{-30}$ and para $L_{30}$ isomers, with the last being very close in its energy to the $E_{11}$ band of the pristine SWCNT. We note that this expectation is corroborated by recent experimental results, displaying just such diversity in emission spectral features.[6,19,20,45] Importantly, for the first two cases, the lowest energy transition contributing to red-shifted emission is optically allowed, in contrast to that of the pristine SWCNT. Thus, the covalent functionalization of SWCNT allows for efficient radiative recombination of the excitons that ordinarily would have recombined nonradiatively in pristine SWCNTs. Insights into the mechanisms that are responsible for such changes in the lowest energy excitonic band make envisioned applications of SWCNTs in optoelectronics, sensing, and imaging technologies more feasible.

## ■ ASSOCIATED CONTENT

### Supporting Information

The Supporting Information is available free of charge on the ACS Publications website at DOI: 10.1021/acs.jpcc.7b09558.

Tables of the total energies and bond lengths calculated with small versus large basis sets, varying functionalization configurations, and chemical species and figures of the total energies for different functionalization configurations calculated with different size basis sets, ground-state molecular orbitals and molecular orbital diagrams for all functionalization configurations using different basis sets, basis set dependence on absorption features for various geometries, total energies of different functionalization configurations calculated with geometries optimized in different solvents, static dipole moments for ground-state aryl-H configurations, natural transition orbitals for different functionalization configurations, and potential energy curves and absorption features for rotation about the dihedral angle of the functional group−SWCNT connectivity for all functionalization configurations (PDF)

## ■ AUTHOR INFORMATION


### Corresponding Author

*(S.T.) E-mail: serg@lanl.gov.

### ORCID

Svetlana Kilina: 0000-0003-1350-2790
Han Htoon: 0000-0003-3696-2896
Stephen K. Doorn: 0000-0002-9535-2062
Sergei Tretiak: 0000-0001-5547-3647


### Notes

The authors declare no competing financial interest.

## ■ ACKNOWLEDGMENTS

This work was conducted, in part, at the Center for Integrated Nanotechnologies, a U.S. Department of Energy, Office of Basic Energy Sciences user facility and supported in part by Los Alamos National Laboratory (LANL) Directed Research and Development Funds. S.K. acknowledges NSF Grant CHE-1413614 for financial support of studies of functionalized carbon nanotubes and the Alfred P. Sloan Research Fellowship BR2014-073 for partial support of studies of surface effects at interfaces of nanostructures. For computational resources and administrative support, S.K. and B.G. thank the Center for Computationally Assisted Science and Technology (CCAST) at North Dakota State University and the National Energy Research Scientific Computing Center (NERSC) allocation awards 86678, supported by the Office of Science of the DOE under Contract No. DE-AC02-05CH11231. We also acknowledge the LANL Institutional Computing (IC) Program for providing computational resources.

## ■ REFERENCES

(1) Saito, R.; Dresselhaus, G.; Dresselhaus, M. S. *Physical Properties of Carbon Nanotubes* **1998**, DOI: 10.1142/p080.

(2) Dass, D.; Prasher, R.; Vaid, R. Analytical Study of Unit Cell and Molecular Structures of Single Walled Carbon Nanotubes. *Int. J. Comput. Eng. Res.* **2012**, *2*, 1447−1457.

(3) Ghosh, S.; Bachilo, S. M.; Simonette, R. A.; Beckingham, K. M.; Weisman, R. B. Oxygen Doping Modifies near-Infrared Band Gaps in Fluorescent Single-Walled Carbon Nanotubes. *Science* **2010**, *330*, 1656−1659.

(4) Piao, Y. M.; Meany, B.; Powell, L. R.; Valley, N.; Kwon, H.; Schatz, G. C.; Wang, Y. H. Brightening of Carbon Nanotube Photoluminescence Through the Incorporation of $sp^3$ Defects. *Nat. Chem.* **2013**, *5*, 840−845.

(5) Ma, X. D.; Hartmann, N. F.; Baldwin, J. K. S.; Doorn, S. K.; Htoon, H. Room-Temperature Single-Photon Generation from Solitary Dopants of Carbon Nanotubes. *Nat. Nanotechnol.* **2015**, *10*, 671−675.

(6) He, X.; Gifford, B.; Hartmann, N. F.; Ihly, R.; Ma, X.; Kilina, S.; Luo, Y.; Shayan, K.; Strauf, S.; Blackburn, J. L.; Tretiak, S.; Doorn, S. K.; Htoon, H. Low Temperature Single Carbon Nanotube Spectros-

copy of sp3 Quantum Defects. *ACS Nano* **2017**, DOI: 10.1021/acsnano.7b03022.
(7) Zhang, D. H.; Ryu, K.; Liu, X. L.; Polikarpov, E.; Ly, J.; Tompson, M. E.; Zhou, C. W. Transparent, Conductive, and Flexible Carbon Nanotube Films and Their Application in Organic Light-Emitting Diodes. *Nano Lett.* **2006**, *6*, 1880−1886.
(8) Bansal, M.; Srivastava, R.; Lal, C.; Kamalasanan, M. N.; Tanwar, L. S. Carbon Nanotube-Based Organic Light Emitting Diodes. *Nanoscale* **2009**, *1*, 317−330.
(9) Mueller, T.; Kinoshita, M.; Steiner, M.; Perebeinos, V.; Bol, A. A.; Farmer, D. B.; Avouris, P. Efficient Narrow-Band Light Emission from a Single Carbon Nanotube P-N Diode. *Nat. Nanotechnol.* **2010**, *5*, 27−31.
(10) Wang, S.; Zeng, Q. S.; Yang, L. J.; Zhang, Z. Y.; Wang, Z. X.; Pei, T. A.; Ding, L.; Liang, X. L.; Gao, M.; Li, Y.; Peng, L. M. High-Performance Carbon Nanotube Light-Emitting Diodes with Asymmetric Contacts. *Nano Lett.* **2011**, *11*, 23−29.
(11) Bahena-Garrido, S.; Shimoi, N.; Abe, D.; Hojo, T.; Tanaka, Y.; Tohji, K. Plannar Light Source Using a Phosphor Screen with Single-Walled Carbon Nanotubes as Field Emitters. *Rev. Sci. Instrum.* **2014**, *85*, 104704.
(12) Hartmann, N. F.; Yalcin, S. E.; Adamska, L.; Haroz, E. H.; Ma, X. D.; Tretiak, S.; Htoon, H.; Doorn, S. K. Photoluminescence Imaging of Solitary Dopant Sites in Covalently Doped Single-Wall Carbon Nanotubes. *Nanoscale* **2015**, *7*, 20521−20530.
(13) Pyatkov, F.; Futterling, V.; Khasminskaya, S.; Flavel, B. S.; Hennrich, F.; Kappes, M. M.; Krupke, R.; Pernice, W. H. P. Cavity-Enhanced Light Emission from Electrically Driven Carbon Nanotubes. *Nat. Photonics* **2016**, *10*, 420−427.
(14) Miyauchi, Y.; Iwamura, M.; Mouri, S.; Kawazoe, T.; Ohtsu, M.; Matsuda, K. Brightening of Excitons in Carbon Nanotubes on Dimensionality Modification. *Nat. Photonics* **2013**, *7*, 715−719.
(15) Kwon, H.; Kim, M.; Meany, B.; Piao, Y.; Powell, L. R.; Wang, Y. Optical Probing of Local pH and Temperature in Complex Fluids with Covalently Functionalized, Semiconducting Carbon Nanotubes. *J. Phys. Chem. C* **2015**, *119*, 3733−3739.
(16) Shiraki, T.; Onitsuka, H.; Shiraishi, T.; Nakashima, N. Near Infrared Photoluminescence Modulation of Single-Walled Carbon Nanotubes Based on a Molecular Recognition Approach. *Chem. Commun.* **2016**, *52*, 12972−12975.
(17) Ma, X.; Adamska, L.; Yamaguchi, H.; Yalcin, S. E.; Tretiak, S.; Doorn, S. K.; Htoon, H. Electronic Structure and Chemical Nature of Oxygen Dopant States in Carbon Nanotubes. *ACS Nano* **2014**, *8*, 10782−10789.
(18) Ma, X.; Baldwin, J. K.; Hartmann, N. F.; Doorn, S. K.; Htoon, H. Solid-State Approach for Fabrication of Photostable, Oxygen-Doped Carbon Nanotubes. *Adv. Funct. Mater.* **2015**, *25*, 6157−6164.
(19) Maeda, Y.; Minami, S.; Takehana, Y.; Dang, J.-S.; Aota, S.; Matsuda, K.; Miyauchi, Y.; Yamada, M.; Suzuki, M.; Zhao, R.-S.; et al. Tuning of the Photoluminescence and up-Conversion Photoluminescence Properties of Single-Walled Carbon Nanotubes by Chemical Functionalization. *Nanoscale* **2016**, *8*, 16916−16921.
(20) Shiraki, T.; Shiraishi, T.; Juhász, G.; Nakashima, N. Emergence of New Red-Shifted Carbon Nanotube Photoluminescence Based on Proximal Doped-Site Design. *Sci. Rep.* **2016**, *6*, 28393.
(21) Kwon, H.; Furmanchuk, A. o.; Kim, M.; Meany, B.; Guo, Y.; Schatz, G. C.; Wang, Y. Molecularly Tunable Fluorescent Quantum Defects. *J. Am. Chem. Soc.* **2016**, *138*, 6878−6885.
(22) Ramirez, J.; Mayo, M. L.; Kilina, S.; Tretiak, S. Electronic Structure and Optical Spectra of Semiconducting Carbon Nanotubes Functionalized by Diazonium Salts. *Chem. Phys.* **2013**, *413*, 89−101.
(23) Kilina, S.; Ramirez, J.; Tretiak, S. Brightening of the Lowest Exciton in Carbon Nanotubes Via Chemical Functionalization. *Nano Lett.* **2012**, *12*, 2306−2312.
(24) Kim, M.; Adamska, L.; Hartmann, N. F.; Kwon, H.; Liu, J.; Velizhanin, K. A.; Piao, Y. M.; Powell, L. R.; Meany, B.; Doorn, S. K.; Tretiak, S.; Wang, Y. H. Fluorescent Carbon Nanotube Defects Manifest Substantial Vibrational Reorganization. *J. Phys. Chem. C* **2016**, *120*, 11268−11276.
(25) Furche, F.; Ahlrichs, R. Adiabatic Time-Dependent Density Functional Methods for Excited State Properties. *J. Chem. Phys.* **2002**, *117*, 7433−7447.
(26) Bahr, J. L.; Yang, J. P.; Kosynkin, D. V.; Bronikowski, M. J.; Smalley, R. E.; Tour, J. M. Functionalization of Carbon Nanotubes by Electrochemical Reduction of Aryl Diazonium Salts: A Bucky Paper Electrode. *J. Am. Chem. Soc.* **2001**, *123*, 6536−6542.
(27) Kim, W. J.; Usrey, M. L.; Strano, M. S. Selective Functionalization and Free Solution Electrophoresis of Single-Walled Carbon Nanotubes: Separate Enrichment of Metallic and Semiconducting Swnt. *Chem. Mater.* **2007**, *19*, 1571−1576.
(28) Nair, N.; Kim, W. J.; Usrey, M. L.; Strano, M. S. A Structure-Reactivity Relationship for Single Walled Carbon Nanotubes Reacting with 4-Hydroxybenzene Diazonium Salt. *J. Am. Chem. Soc.* **2007**, *129*, 3946−3954.
(29) Usrey, M. L.; Lippmann, E. S.; Strano, M. S. Evidence for a Two-Step Mechanism in Electronically Selective Single-Walled Carbon Nanotube Reactions. *J. Am. Chem. Soc.* **2005**, *127*, 16129−16135.
(30) Frey, J. T.; Doren, D. J., Tubegen 3.4; University of Delaware: Newark, DE, 2011.
(31) Kilina, S.; Tretiak, S. Excitonic and Vibrational Properties of Single-Walled Semiconducting Carbon Nanotubes. *Adv. Funct. Mater.* **2007**, *17*, 3405−3420.
(32) Sharma, A.; Gifford, B. J.; Kilina, S. Tip Functionalization of Finite Single-Walled Carbon Nanotubes and Its Impact on the Ground and Excited State Electronic Structure. *J. Phys. Chem. C* **2017**, *121*, 8601−8612.
(33) Rappe, A. K.; Casewit, C. J.; Colwell, K. S.; Goddard, W. A.; Skiff, W. M. UFF, a Full Periodic-Table Force-Field for Molecular Mechanics and Molecular-Dynamics Simulations. *J. Am. Chem. Soc.* **1992**, *114*, 10024−10035.
(34) Dewar, M. J. S.; Zoebisch, E. G.; Healy, E. F.; Stewart, J. P. Am1: A New General Purpose Quantum Mechanical Molecular Model. *J. Am. Chem. Soc.* **1985**, *107*, 3902−3909.
(35) Yanai, T.; Tew, D. P.; Handy, N. C. A New Hybrid Exchange−Correlation Functional Using the Coulomb-Attenuating Method (CAM-B3LYP). *Chem. Phys. Lett.* **2004**, *393*, 51−57.
(36) Kilina, S.; Badaeva, E.; Piryatinski, A.; Tretiak, S.; Saxena, A.; Bishop, A. R. Bright and Dark Excitons in Semiconductor Carbon Nanotubes: Insights from Electronic Structure Calculations. *Phys. Chem. Chem. Phys.* **2009**, *11*, 4113−23.
(37) Kilina, S.; Kilin, D.; Tretiak, S. Light-Driven and Phonon-Assisted Dynamics in Organic and Semiconductor Nanostructures. *Chem. Rev.* **2015**, *115*, 5929−5978.
(38) Frisch, M. J.; Trucks, G. W.; Schlegel, H. B.; Scuseria, G. E.; Robb, M. A.; Cheeseman, J. R.; Scalmani, G.; Barone, V.; Mennucci, B.; Petersson, G. A.; et al. *Gaussian 09*; Gaussian, Inc.: Wallingford, CT, 2009.
(39) Cossi, M.; Rega, N.; Scalmani, G.; Barone, V. Energies, Structures, and Electronic Properties of Molecules in Solution with the C-PCM Solvation Model. *J. Comput. Chem.* **2003**, *24*, 669−681.
(40) Van Caillie, C.; Amos, R. D. Geometric Derivatives of Density Functional Theory Excitation Energies Using Gradient-Corrected Functionals. *Chem. Phys. Lett.* **2000**, *317*, 159−164.
(41) Martin, R. L. Natural Transition Orbitals. *J. Chem. Phys.* **2003**, *118*, 4775−4777.
(42) Wongchoosuk, C.; Udomvech, A.; Kerdcharoen, T. The Geometrical and Electronic Structures of Open-End Fully Functionalized Single-Walled Carbon Nanotubes. *Curr. Appl. Phys.* **2009**, *9*, 352−358.
(43) Kilina, S.; Tretiak, S.; Doorn, S. K.; Luo, Z.; Papadimitrakopoulos, F.; Piryatinski, A.; Saxena, A.; Bishop, A. R. Cross-Polarized Excitons in Carbon Nanotubes. *Proc. Natl. Acad. Sci. U. S. A.* **2008**, *105*, 6797−6802.
(44) Wu, C.; Malinin, S.; Tretiak, S.; Chernyak, V. Exciton Scattering and Localization in Branched Dendrimeric Structures. *Nat. Phys.* **2006**, *2*, 631−635.


DOI: 10.1021/acs.jpcc.7b09558
*J. Phys. Chem. C* 2018, 122, 1828−1838

(45) He, X.; Hartmann, N. F.; Ma, X.; Kim, Y.; Ihly, R.; Blackburn, J. L.; Gao, W.; Kono, J.; Yomogida, Y.; Hirano, A.; et al. Tunable Room-Temperature Single-Photon Emission at Telecom Wavelengths from sp3 Defects in Carbon Nanotubes. *Nat. Photonics* **2017**, *11*, 577−582.



DOI: 10.1021/acs.jpcc.7b09558
*J. Phys. Chem. C* 2018, 122, 1828−1838